Journal of Molecular Catalysis A: Chemical 377 (2013) 197–203

Contents lists available at SciVerse ScienceDirect

Journal of Molecular Catalysis A: Chemical

journal homepage: www.elsevier.com/locate/molcata

Photolysis and photocatalysis of methylene blue by ferrite bismuth nanoparticles under sunlight irradiation

Tayyebe Soltani, Mohammad H. Entezari*

Department of Chemistry, Ferdowsi University of Mashhad, 91775 Mashhad, Iran

ARTICLE INFO

Article history:
Received 28 March 2013
Received in revised form 2 May 2013
Accepted 11 May 2013
Available online xxx

Keywords:
Ultrasound
$BiFeO_3$
Sunlight irradiation
Photodegradation
Methylene blue

ABSTRACT

Ferrite bismuth nanoparticles as a visible light photocatalyst were successfully synthesized via ultrasound. The optimum conditions were found and applied for the sono-synthesis of the catalyst. The product was characterized by different methods. The nanoparticles were used for the degradation of methylene blue as a typical dye pollutant. In acidic medium, the photocatalytic degradation was carried out under direct sunlight irradiation. In basic medium, without catalyst, the methylene blue was degraded through photolysis under sunlight irradiation. The effect of parameters such as the amount of catalyst and initial concentration of the dye was investigated on the removal efficiency of methylene blue. The adsorption isotherm and the kinetic of photocatalytic degradation were studied under different conditions. Furthermore, the degradation efficiency and the chemical oxygen demand reduction were 100% and 83% for the photocatalytic process, respectively.

1. Introduction

Dyes are widely used in industries such as textile, rubber, paper, plastic, and cosmetic. During the dyeing process, high amount of the total world production of dyes discharge into the waters every day [1]. This causes serious environmental problems such as increase of toxicity, chemical oxygen demand (COD), biochemical oxygen demand (BOD), bad smell, and color of the water [2]. Non-destructive conventional water treatment such as adsorption, coagulation, flocculation, reverse osmosis and ultrafiltration just transfer contaminants from one phase to another phase and form secondary waste problems [3].

Methylene blue (MB) is a blue cationic thiazine dye with λ_{max} values at 662, 614 and 292 nm [4]. It contains three mesomeric structures in which the positive charge can be placed either on the amine nitrogen atom or on the sulfur atom [5]. The reduced forms of MB, Leuco-methylene blue (LMB) (λ_{max} = 256, 322 nm) [6] and MBH_2^+ (λ_{max} = 232 nm) [7] are colorless and stable in aqueous solution. MB is blue in an oxidizing environment and readily reduced to the colorless, leuco forms, by reducing agents [8].

Nowadays, advance oxidation processes (AOPs) are successfully employed for the complete mineralization of organic pollutants in water [9]. In these processes, photogenerated holes and reactive species such as hydroxyl radicals in a semiconductor could oxide a broad range of organic pollutants quickly and non-selectively to inorganic substances such as Cl^-, SO_4^{2-} and NO_3^- [10].

TiO_2 as a photocatalyst can only be activated under UV light irradiation (λ < 380 nm) due to its large band gap energy (3.2 eV) [11]. Hence, development of non-titania semiconductors with strong absorbance in the visible region is very important.

Ferrite bismuth $BiFeO_3$ (BFO) with a rhombohedrally distorted perovskite structure is a new important visible-light photocatalyst for the degradation of organic pollutants due to its narrowing band gap energy (2.2 eV) and excellent chemical stability [12–14]. This photocatalysis is quite different from most of the narrow energy band gap that suffer from unstable enough against the photocorrosion such as CdS [15]. Furthermore, it is famous as a well-known multiferric compound that demonstrates the coexistence of ferroelectric and antiferromagnetic order above room temperature with Neel temperature (T_N ~375 °C) and Curie temperature (T_C ~830–850 °C). It is cubic above and rhombohedrally below its Curie temperature [16,17]. The BFO nanoparticles exhibit a weak ferromagnetic (FM) order at room temperature that is quite different from the linear magnetization–magnetic field relationship in the bulk [18].

Today, many research groups have developed various methods to prepare pure BFO nanoparticles [19–21]. The synthesis of BFO by various methods often is complex and performs at high temperature (800 °C) which lead to impurity phases such as Bi_2O_3, Fe_2O_3, and $Bi_2Fe_4O_9$ [22,19]. For example, some impurities like $Bi_{36}Fe_{24}O_{57}$ and $Bi_2Fe_4O_9$ can be existed in the nanoparticles synthesized by a sol–gel method, when $Bi(NO_3)_3{\cdot}5H_2O$ and $Fe(NO_3)_3{\cdot}9H_2O$ dissolved in 2-methoxyethanol and annealed at

* Corresponding author. Fax: +98 511 8795457.
E-mail address: moh_entezari@yahoo.com (M.H. Entezari).

1381-1169/$ – see front matter © 2013 Elsevier B.V. All rights reserved.
http://dx.doi.org/10.1016/j.molcata.2013.05.004

600 °C for 30 min [23]. Another phase such as $Bi_{25}FeO_{40}$ appeared in the powders synthesized by hydrothermal method [24]. Traditional solid state route, using Bi_2O_3 and Fe_2O_3 as reactants, needs high calcination temperature (above 800 °C) and the unavoidable impurities must be removed by leaching in the diluted nitric acid [25–27]. Thus, preparation of pure phase BFO is still a great challenge, and it is not possible to prepare the structure-controllable BFO nanoparticles with high surface area [28,29].

By ultrasound, it is possible to synthesize the pure nanoparticles under normal conditions without additives, and avoiding calcinations at high temperatures [30]. The high speed microjet which results from cavitation produce enormous energy that could improve the chemical and physical properties of the materials [31]. The sono-synthesis of semiconductors [32–34], sonophotocatalytic, sonocatalytic, and photocatalytic degradation of dyes have been carried out in our lab [35,36].

In this work, the BFO nanoparticles synthesized via ultrasound applied for the degradation of MB as a representative dye pollutant of the textile wastewaters.

2. Experimental

2.1. Chemical and materials

Bismuth nitrate ($Bi(NO_3)_3{\cdot}5H_2O$), iron nitrate ($Fe(NO_3)_3{\cdot}9H_2O$), ethylene glycol (EG) and MB from Merck have been used without further purification. Ethanol and de-ionized water were used for the sample preparation.

2.2. Catalyst preparation

First, to form a transparent solution, 0.008 mol bismuth nitrate ($Bi(NO_3)_3{\cdot}5H_2O$) was sonicated in EG for 15 min. At the end of sonication time, the temperature was increased from 9 to 35 °C. Then, the stoichiometric proportion of iron nitrate ($Fe(NO_3)_3{\cdot}9H_2O$) was added into the solution. The mixture was sonicated for another 10 min at the same temperature to obtain a brownish red sol. Then the samples were kept at 70 °C to form a xerogel powder. The obtained powders were calcinated at different temperatures. Finally, the powders washed with distilled water and absolute alcohol for several times and dried at 70 °C.

2.3. Characterization and equipment

The crystalline structure was identified by X-ray diffraction (XRD) (Philips PW1800) employing Cu Kα ($\lambda = 1.5406$ Å, $2\theta = 10$–80°). The sizes of the samples were determined with transmission electron microscope (TEM, Leo 912 AB). The light absorption strength of the nanoparticles was analyzed by UV–vis diffuse reflectance spectra (DRS, MC-2530). The concentration of MB was measured by using UV–vis spectrophotometer (model Unico 2800) and the COD was determined under different conditions [37].

The ultrasonic irradiation was performed with equipment operating at 20 kHz (Branson Digital sonifier, Model W-450 D).

2.4. Sunlight irradiation

The photocatalytic degradation of MB has been investigated under direct solar irradiation with sample synthesized by ultrasound. In this case, several glass vessels containing 100 mL MB (15 mg L^{-1}) and appropriate quantity of photocatalyst (0.5 g L^{-1}) were magnetically stirred at 720 rpm on the window ledge under direct solar radiation in consecutive sunny days in July 2012 between 11.30 AM and 2 PM (GPS coordinates: N = 36°18′41.6″, E = 59°31′54.2″). All experiments were carried out at temperature between 28 and 32 °C. Before illumination, the solution was magnetically stirred in dark for 60 min to attain adsorption–desorption equilibrium between the dye and photocatalyst.

Different amounts of catalyst (0.25–1.00 g L^{-1}) were tested (Fig. S1) for the degradation of 100 mL MB (15 mg L^{-1}) and the best dosage was selected (0.50 g L^{-1}). The higher dosage of catalyst may not be useful because of aggregation as well as reducing the irradiation field due to light scattering [38]. At appropriate time intervals, about 5 mL of suspension was sampled and the solid phase was separated from the solution with an external magnetic field. The removal of MB was determined based on the absorption at 662 nm by using a UV–vis spectrophotometer. Then, the absorption was converted to the concentration through the standard curve (information supporting Fig. S2).

Some other experiments under different pH were also carried out by adding HCl or NaOH to the solution.

3. Results and discussion

3.1. Characterization of the catalyst

3.1.1. XRD results

Fig. 1 shows the XRD patterns of the xerogel dried at 70 °C and the powders calcinated at different temperatures. The powder at 70 °C is amorphous but, with heating to 180 °C, some weak peaks was formed which are related to the bismuth oxide (Bi_2O_3) and other impurities. The intensity of peaks was enhanced with increasing the calcination temperature to 400 °C. When the sample was remained at 500 °C for 1 h, the XRD analysis showed only the pattern corresponding to the rhombohedral structure of BFO with *R*3*c* space group (JCPDS no: 71-2494). The slight splitting of peak at $2\theta = 32$ confirms the rhombohedral symmetry of BFO. Furthermore, the width of the BFO peaks increases when the sample was remained at 400 °C for 0.5 h and then at 500 °C for another 0.5 h. Based on the Debye–Scherrer formula, the average crystalline size according to the (0 1 2) diffraction peak for the sample calcinated at 500 °C for 1 h was 58.12 nm and for the sample calcinated at 400 °C for 0.5 h and then at 500 °C for another 0.5 h was 40.12 nm. Therefore, the last calcination temperature program was applied for the synthesis of the catalyst.

At lower calcination temperatures (200 and 300 °C), the BFO had no activity. The nanoparticles calcinated at 500 °C for 1 h, were impure and had a lower photocatalytic activities than the sample calcinated at 400 °C for 0.5 h and then at 500 °C for another 0.5 h

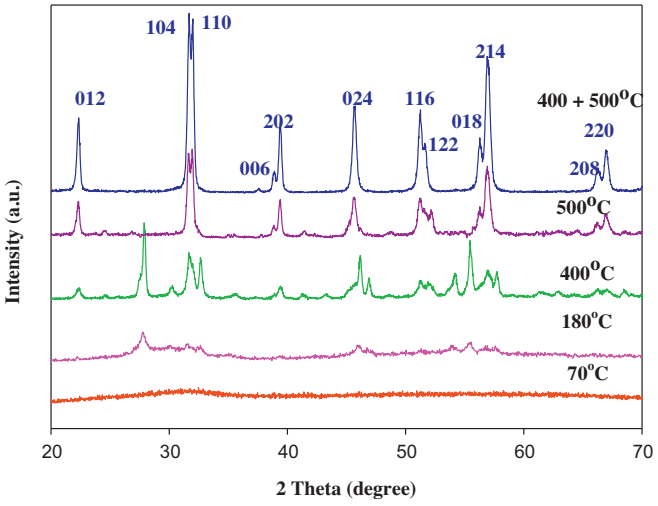

Fig. 1. XRD patterns of dried xerogel and dried xerogel that remaining at different calcination temperatures for 1 h.

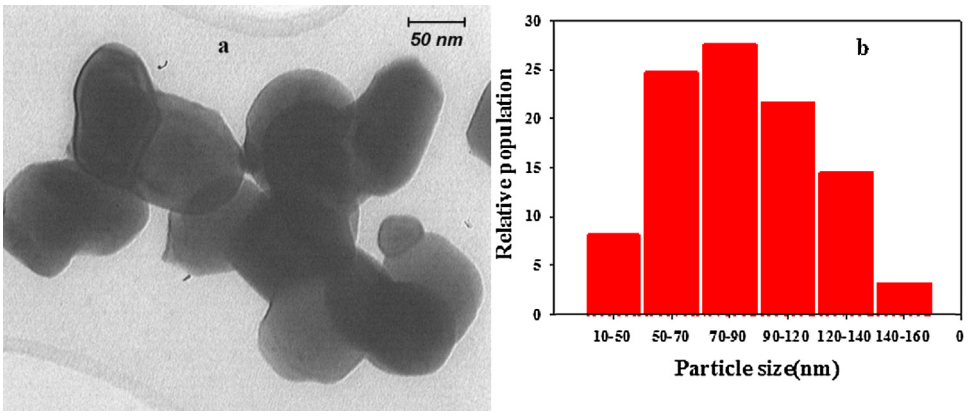

Fig. 2. (a) TEM and (b) particle size distribution of BFO nanopowders.

(not shown). The higher calcination temperatures of 600, 700 and 800 °C (1 h) were also checked. These nanoparticles were not pure the same as other results [23,25–27]. In addition, these nanoparticles exhibited lower photocatalytic activities for the degradation of MB (not shown). This behavior can be related to the some impurities and also higher crystallite size of these nanoparticles [28,29]. Thus, the sample in this work was calcinated at two different temperatures (400 and 500 °C) for 0.5 h and then applied for the degradation of MB.

For comparison, another sample was synthesized via sol–gel method at high temperature and long time (3.5 h) [14]. The nanoparticles synthesized with sol–gel method under stricter conditions, exhibited some impurities such as Bi_2O_3 the same as other results [22,19,23–27]. This kind of impurity shows a deactivation of BFO nanoparticles [39]. The XRD patterns of the nanoparticles are shown in Fig. S3 in the information supporting. Furthermore, the nanoparticles had higher crystallite size and lower photocatalytic activity than the sample synthesized with ultrasonic method (not shown).

During the acoustic cavitation process, very high temperatures (>5000 K), pressures (>20 MPa), and cooling rates (>10^{10} K s^{-1}) can be obtained upon the collapse of the bubbles which provide a favorable environment for the growth of the nanocrystals [30,31]. In addition, these nanoparticles have smaller crystallite size. This means that the number of sorption sites and radical species increase for the nanoparticles synthesized via ultrasound [40].

Fig. 2 shows the TEM image and size distribution of BFO nanoparticles which are nearly spherical.

3.1.2. Optical performance of BFO

According to the UV–vis DRS spectrum (Fig. 3), the BFO nanoparticles have a strong visible-light absorption which is related to the band gap energy of the photocatalyst. As shown in the inset of Fig. 3, the band-gap energy can be calculated by using $(ahv)^n = B(hv - E_g)$, where a, h, v, E_g and B are absorption coefficient, Planck constant, light frequency, band gap energy, and a constant, respectively [41]. The corresponding band gap energy was about 2.17 eV, by extrapolating the linear portion of $(\alpha hv)^2$ against hv plot to the point $a = 0$. Based on calculation, the band gap energy was comparable with previous results [42]. Thus, BFO nanoparticles exhibited a strong potential application as an appropriate photocatalyst for the degradation of materials in the visible region.

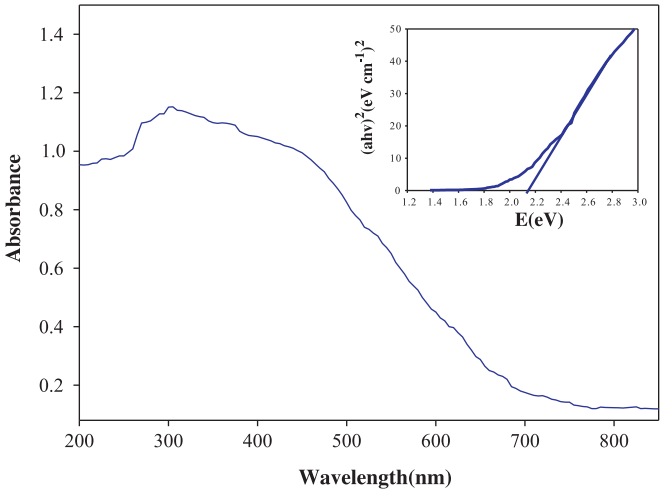

Fig. 3. UV–vis DRS spectrum of BFO nanoparticle synthesized via ultrasound, the inset shows the calculation of the band gap energy.

3.2. Degradation of MB

3.2.1. Photo-degradation

3.2.1.1. Effect of pH. The solutions of MB without BFO in various initial pH values from 2.5 to 12.0 were left in a dark place for 60 min. The dye removal efficiency was negligible in all selected pH. Then, the dye solutions were exposed to sunlight irradiation and different behaviors were observed as shown in Fig. 4. At natural and acidic media, there was no decrease in the concentration of dye. This indicates that the direct photolysis of MB by solar irradiation was negligible at these media. It means that, excitation of dye molecules by photon and then dispersion of their excitation energy had no role on the decolorization of the dye (reaction (1)):

$$\text{Dye} + hv \rightarrow \text{NO Products} \quad (1)$$

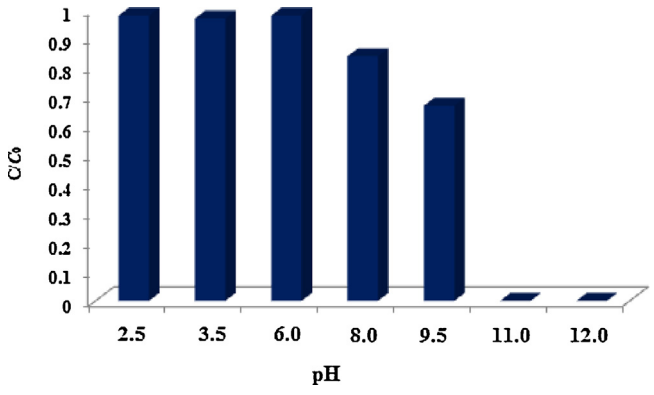

Fig. 4. Photolysis of MB at different pH (C_0 = 15 mg L^{-1}, time of irradiation = 90 min).

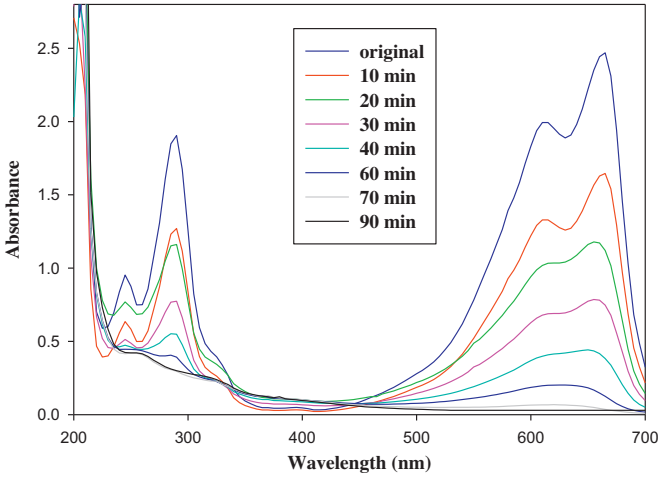

Fig. 5. Photolysis of MB at pH = 11.0 (temp., 32 °C, mixing rate, 720 rpm).

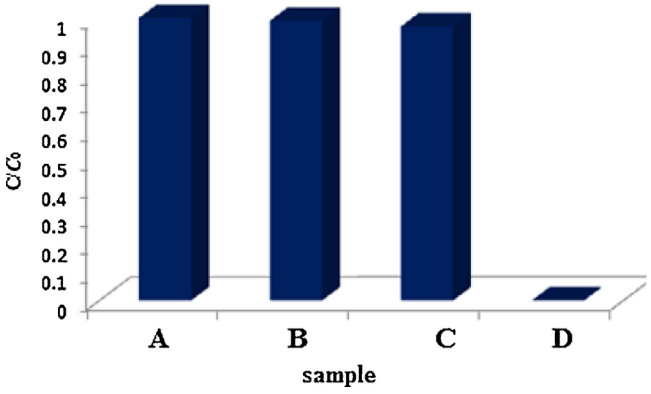

Fig. 6. Photolysis of MB at pH = 11.0 (temp., 32 °C; mixing rate, 720 rpm, C_0 = 15 mg L^{-1}): (A) original dye, (B) dye in dark for 90 min, (C) dye in light for 90 min (Ar saturated solution), and (D) dye in light for 90 min (in the presence of air).

But, with increasing the hydroxyl ions, the rate of photolysis was rapidly increased (reaction (2)):

$$\text{Dye} + h\nu \xrightarrow{OH^-} \text{Products} \quad (2)$$

A complete photolysis of MB was obtained at pH values of 11 and 12 in 90 and 30 min, respectively.

3.2.1.2. Photolysis at basic medium. Fig. 5 shows UV–vis absorption spectra of MB in aqueous solution at different interval times of irradiation (pH = 11.0). The absorption peaks between 600 and 700 nm can be attributed to a chromophore containing a long conjugated π system, while the absorption peak at 292 nm can be related to the aromatic rings [43]. According to Fig. 5, the absorption peaks decrease considerably throughout the irradiation time and finally disappear after 90 min of sunlight irradiation.

Fig. S4 (information supporting) shows the change of initial pH from 11.0 to 9.2 after 90 min of sunlight irradiation. This behavior could be related to the subsequent proton-producing reactions, formation of nitrate and sulfate ions (reaction (3)) [44]:

$$C_{16}H_{18}N_3S^+ + \tfrac{15}{2}O_2 \rightarrow 16CO_2 + 3NO_3^- + SO_4^{2-} + 6H^+ + 6H_2O \quad (3)$$

The final degradation of MB leads to carbon dioxide, sulfate, nitrate, and ammonium ions from carbon, sulfur and nitrogen heteroatoms, respectively [45,46].

3.2.1.3. Photolysis mechanism. Some experiments were performed without BFO at pH = 11.0 to investigate the mechanism of photolysis. The dye removal efficiency after 90 min in a dark place at 32 °C was negligible (Fig. 6B).

In another experiment, the temperature was raised to 40 °C and the other variables remained constant. In this case, the photolysis was negligible too. Thus, the temperature has no essential role on the photolysis of MB. One experiment was carried out under Ar atmosphere (Fig. 6C). The results showed that the photolysis of MB was completely stopped under Ar atmosphere. But, at the air atmosphere, the photolysis of MB was complete after 90 min of sun light irradiation (Fig. 6D). It means O_2 has an essential role on the photolysis of MB. Thus, light, O_2, and OH^- have major effects on the photolysis as it can be stopped with lack of any of them.

Some information were reported from ESR spectroscopy results about radicalic species formed during the photolysis of MB in acidic and basic aqueous solutions [47]. In basic aqueous solutions under solar light irradiations, highly reactive hydroxyl radicals can be formed through monoelectronic reduction of MB^+ by the hydroxyl ion [48] (reactions (4)):

$$MB^+ + OH^- \rightarrow MB^\bullet + OH^\bullet \quad (4)$$

Hydroxyl radical species can react with each others and producing H_2O_2 which is an important active species in degradation processes (reaction (5)).

$$2OH^\bullet \rightarrow H_2O_2 \quad (5)$$

Oxygen as a radical scavenger can react with $MB^\bullet$ radical and form $O_2{}^{-\bullet}$ as another important intermediate species according to the reaction (6) [49].

$$MB^\bullet + O_2 \rightarrow MB^+ + O_2{}^{-\bullet} \quad (6)$$

Thus, the photolysis of MB at basic media could be preceded via direct reactions of MB with highly reactive radical species that formed in the presence of sunlight irradiation.

3.2.2. Photocatalytic degradation

3.2.2.1. Effect of pH. One of the most important parameter that influences the photocatalytic degradation of dye is pH. This is due to the effect of pH on the surface-charge-properties of the photocatalyst and the influences on the ionic species in the solution. Therefore, the effects of pH were investigated on the photocatalytic activity of BFO. Different experiments were performed at pH values of 2.5, 3.5, 6.0, 8.0, 9.5, 11.0 and 12.0 as shown in Fig. 7. The dye concentration was constant (15.0 mg L^{-1}) and the dose of catalyst was fixed at 0.5 g L^{-1}. Before illumination, the suspensions were stirred at dark place for 60 min to reach an adsorption–desorption equilibrium between the photocatalyst and MB (inset of Fig. 7). Then, the suspensions were exposed to sunlight irradiation for another 90 min (Fig. 7).

At equilibrium in dark (60 min), approximately 53% of MB was adsorbed on the surface of catalyst at pH = 2.5. But, under sunlight irradiation, it was completely degraded. With increasing the pH to 3.5, approximately 40% of MB was adsorbed by catalyst in dark and 80% was degraded after 90 min of sunlight irradiation. When the pH increased to 6.0, the adsorption and degradation were negligible. In dark place, the catalyst had no adsorption in basic media (8.0, 9.5, 11.0 and 12.0). But, the results show that the removal efficiency of MB was higher in both acidic and basic media rather than near the neutral medium under sunlight irradiation (Fig. 7).

The comparison of the pH results (with and without BFO) showed that the mechanism of degradation of MB in acidic and basic media is different. The basic medium could not be useful in the photocatalytic degradation of MB and only the photolysis can be responsible for the degradation. In addition, with increasing the

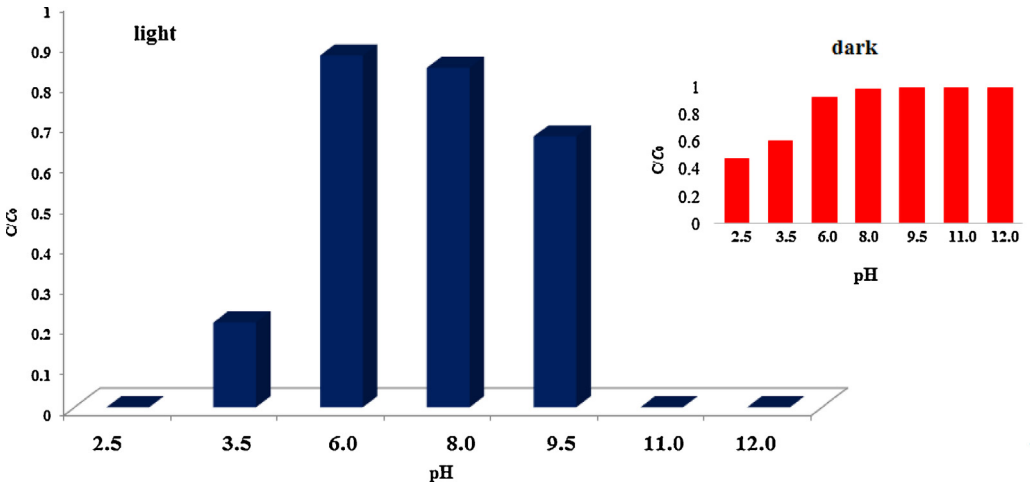

Fig. 7. Degradation efficiency of MB at different pH under sun light irradiation after 90 min, inset: adsorption of MB during 60 min in dark (temp., 32 °C; C_0 = 15 mg L^{-1}, dose of catalyst = 0.5 g L^{-1}, mixing rate = 720 rpm).

pH from 8.0 to 12.0, the time of complete photolysis was decreased too. But, the photocatalytic degradation of MB was carried out in aqueous solution by BFO nanoparticles at acidic media and the best results were achieved at pH = 2.5.

3.2.2.2. Photocatalysis at acidic medium. At first, the suspensions were stirred at dark place for 60 min to reach an adsorption–desorption equilibrium between the photocatalyst and MB, then, the suspensions were placed in the presence of sunlight irradiation for different interval times. The photocatalytic activities of BFO nanoparticles were studied for the degradation of MB in acidic medium under sunlight irradiations (Fig. 8).

Based on Fig. 8, the adsorption peaks at 290 and 660 nm which are attributed to the aromatic rings and conjugated structure decreased considerably as the time of irradiation increased and finally disappeared after 80 min of irradiation. In addition, the results of desorption test from the surface of BFO (not shown) confirmed that nearly 95% of MB, was degraded and just 5% remained on the surface of BFO after 80 min of sunlight irradiation.

The stability and the reusability of nanoparticles were checked for several times. In each cycle, in the presence of sunlight irradiation, the suspension was magnetically stirred for 80 min. Then, the suspension was separated from the solution by an external magnetic field and again, 100 mL of original dye solution of MB (15 mg L^{-1}) was added to the separated solid phase. This experiment was repeated four times. The results showed that no decrease in degradation efficiency was observed in successive cycles. Thus, the photocatalyst was stable and active under visible light after several successive cycles (Fig. S5). The FT-IR results also confirmed this claim (Fig. S6).

3.2.2.3. Photocatalytic degradation mechanism. The mechanism of photocatalytic degradation of MB has been checked through the addition of some scavengers (isopropanol as a scavenger of $OH^{\bullet}$ radicals, potassium iodide as a quencher of positive hole and $OH^{\bullet}$) into the solution. The results showed that the hole as a reactive species had a key role in the degradation process of MB at acidic medium (not shown). Therefore, it assumed that after adsorption of MB on the surface of BFO at dark, the photocatalytic degradation of MB under sun light irradiation could be preceded via direct reactions of MB with holes trapped on the surface.

3.2.2.4. Reduction of COD in acidic medium. The removal efficiency of COD in solution, on the surface, and the total, were examined at different interval times at pH = 2.5. The results are shown in Fig. 9. The COD was measured by dichromate method [7]. The COD of adsorbed species on the catalyst was measured through desorption of species from the surface by dispersing the catalyst in an aqueous solution at basic medium (pH = 10). The solution was

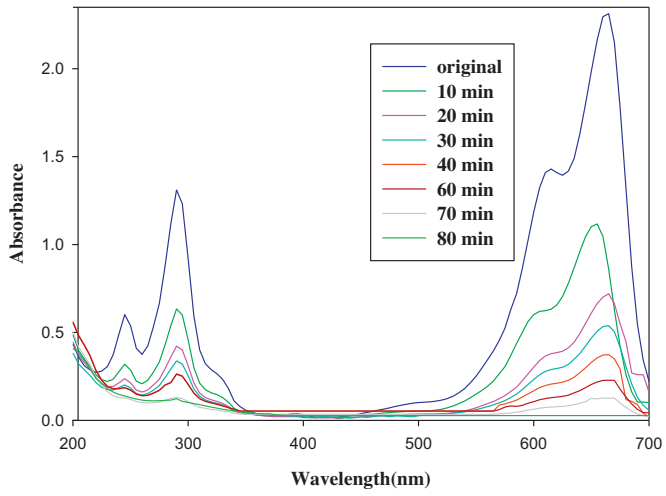

Fig. 8. Photocatalytic degradation of MB at pH = 2.5 (temp., 32 °C; dose of catalyst = 0.5 g L^{-1}, mixing rate = 720 rpm).

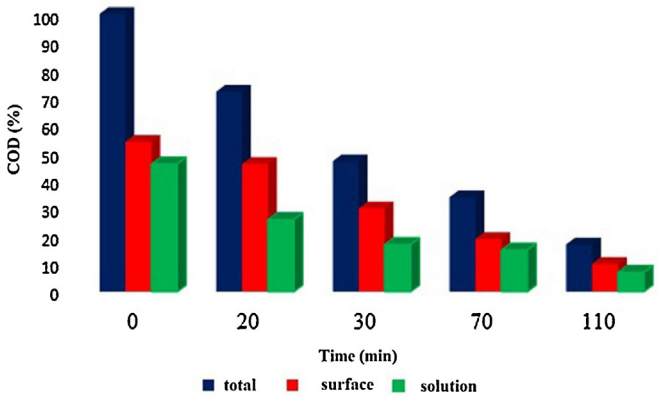

Fig. 9. Removal efficiencies of COD by BFO/light at acidic pH (2.5) (temp., 32 °C; C_0 = 15 mg L^{-1}, dose of catalyst = 0.5 g L^{-1}, mixing rate = 720 rpm).

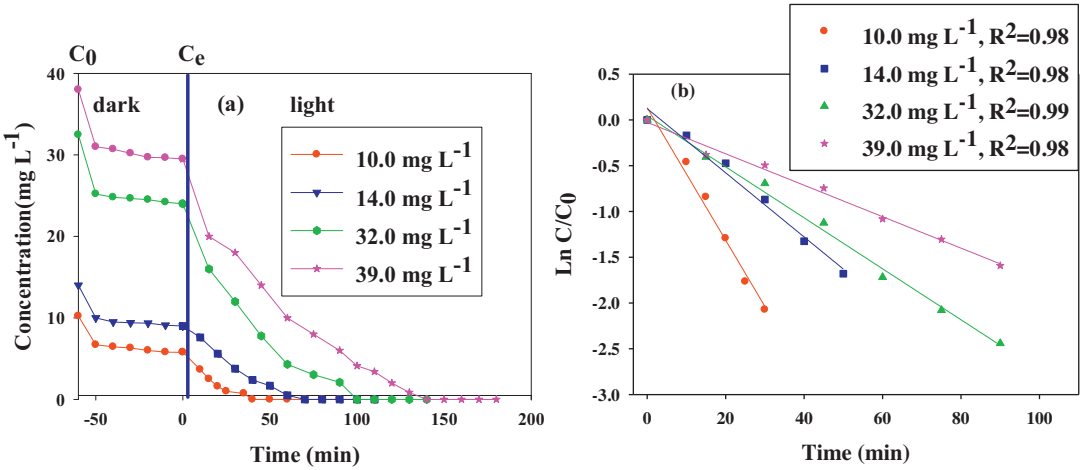

Fig. 10. (a) Effect of initial dye concentration on the degradation of MB and (b) kinetics of photocatalytic degradation of MB with different initial concentrations at pH = 2.5 (temp., 32 °C; dose of catalyst = 0.5 g L^{-1}, mixing rate = 720 rpm).

sonicated for 30 min in ultrasonic bath for complete desorption. The COD at time zero is related to the remained dyes in liquid and on the surface of BFO after reaching the equilibrium in dark. The COD decreased with increasing the time of irradiation. After 110 min, the COD reached to 7%, 10% and 17%, in solution, on the surface, and the total, respectively. The experimental data proved that most of the dye in solution and on the surface was completely mineralized in the photocatalytic degradation process.

As the results show, the photocatalytic degradation efficiency and the photolysis efficiency are clearly higher than the COD removal efficiency. This is due some intermediates that formed during the mineralization of MB on the surface and in the solution.

3.3. Adsorption isotherm

The adsorption of organic molecules on the surface of catalyst exhibits an important role on the photocatalytic process. Therefore, it is important to determine the adsorption isotherm in darkness by using various concentrations of the dye to evaluate the equilibrium constants of the adsorption. The catalyst had no adsorption in basic medium (8.0, 9.5, 11.0 and 12.0). When the pH decreased from 12.0 to 6.0, a little adsorption observed on the surface of catalyst. There was a higher adsorption at acidic media (3.5 and 2.5) that is appropriate to higher photocatalytic activity in these media.

The linear form of the Langmuir model [50] is represented by Eq. (7):

$$\frac{C_e}{q_e} = \left(\frac{1}{q_m K}\right) + \left(\frac{1}{q_m}\right) C_e \tag{7}$$

where q_e (mg g^{-1}), the amount of dye adsorbed on the surface of photocatalyst at equilibrium, c_e (mg L^{-1}), the concentration of dye in solution at equilibrium, K (L mg^{-1}), the equilibrium constant, and q_m (mg g^{-1}) is the maximum amount of dye adsorbed on the photocatalyst.

According to Eq. (7), a plot of (c_e/q_e) versus c_e is shown in Fig. S7 for all of concentrations at pH values of 2.5, 3.5 and 6.0. The values of K and q_m can be obtained via its intercept and slope, respectively.

The calculated values of the equilibrium constant are K = 0.0914 L mg^{-1}, 0.0439 L mg^{-1} and 0.0065 L mg^{-1} for pH 2.5, 3.5 and 6.0, respectively. In addition, the maximum adsorption (q_m) increased from 15.53 mg g^{-1} to 22.28 mg g^{-1} and 23.83 mg g^{-1} with decreasing the pH values from 6.0 to 3.5 and 2.5, respectively. These results confirm that high adsorption and degradation efficiency at pH = 2.5.

3.4. Kinetics of photocatalytic degradation

Fig. 10 presents the effect of various initial concentrations of dye from 10.0 to 38.0 mg L^{-1} on the photocatalytic degradation efficiency. As shown in Fig. 10, with increasing the concentration, the maximum amount of adsorption on the surface was increased and more time is required for complete degradation under sunlight irradiation. In addition, at high concentrations of dye, solar light may be absorbed by the dye itself. Thus, fewer photons reached on the surface of the photocatalyst and lower radical species formed during the irradiation [51].

The photocatalytic degradation of MB obeys the pseudo-first-order kinetic in terms of modified Langmuir–Hinshelwood (L–H) model by Eq. (8):

$$r = -\frac{dc}{dt} = \frac{k_r k_{LH} c}{1 + K_{LH} c} \tag{8}$$

In this equation, r (mg L^{-1} min^{-1}), k_r (mg L^{-1} min^{-1}), K_{LH} (L mg^{-1}), c (mg L^{-1}) and t (min) are the reaction rate, reaction rate constant, adsorption constant, reactant concentration and time of irradiation, respectively [40–52]. At low initial dye concentration, the rate expression (Eq. (8)) can be written in the form of Eq. (9):

$$r = -\frac{dc}{dt} = k_r k_{LH} c = kc \tag{9}$$

where k is the pseudo-first-order rate constant and by integration of Eq. (9) with the limit of $c = c_0$ at $t = 0$, it changes to Eq. (10):

$$\ln\frac{c}{c_0} = -kt \tag{10}$$

In Eq. (10), c_0 is the initial concentration and c is the summation of surface and solution concentrations of dye at each time. According to Eq. (10), the plot of $\ln(c/c_0)$ versus t for all concentrations should be linear and the values of k (k_{app}) can be obtained directly via its slope (Fig. 10 b). The obtained values of k_{app} are equal to 0.0723 min^{-1}, 0.0350 min^{-1}, 0.0270 min^{-1} and 0.0171 min^{-1} for initial concentrations of 10.0 mg L^{-1}, 14.0 mg L^{-1}, 32.0 mg L^{-1} and 39.0 mg L^{-1}, respectively. Therefore, the initial concentration of MB has a significant effect on the degradation rates, as the rate constant of degradation is higher when the initial concentration is lower.

4. Conclusion

In this work, pure BFO nanoparticles as an effective photocatalyst for the degradation of MB under sunlight irradiation, have been successfully synthesized via ultrasound at low temperature

and short time. The nanoparticles with small crystallite size and strong visible-light absorption were appropriate for the photocatalytic degradation of MB. The effect of pH was investigated in details on the photolysis and photocatalysis of MB. The catalyst showed a high adsorption in acidic medium that is appropriate for the complete photocatalytic degradation at low pH. Based on UV–vis spectrum, after 80 min of sunlight irradiation in acidic medium, all peaks disappeared and no new peaks observed. During this time, the relative concentration of dye on the surface was also negligible. The kinetics of photocatalytic degradation of MB was investigated, suggesting a pseudo first-order kinetics model. The reduction in the chemical oxygen demand (COD, 83%) proves the mineralization of the MB along with the color removal. In basic medium, the degradation of MB takes place by only photolysis of dye in the presence of sunlight irradiation. At high pH (12), a complete photolysis takes place in 30 min of irradiation.

Acknowledgement

The support of Ferdowsi University of Mashhad (Research and Technology) for this work (code 3/19022, date 2011/10/19) is appreciated.

Appendix A. Supplementary data

Supplementary data associated with this article can be found, in the online version, at http://dx.doi.org/10.1016/j.molcata.2013.05.004.

References

[1] T. Robinson, G. McMullan, R. Marchant, P. Nigam, Biores. Technol. 77 (2001) 247–255.
[2] A.B. Dos Santos, F.J. Cervantes, J.B. Van Lier, Biores. Technol. 98 (2007) 2369–2385.
[3] Y.M. Slokar, A.M. Le Marechal, Dyes Pigments 37 (1998) 335–356.
[4] N.R. De Tacconi, J. Carmona, K. Rajeshwar, J. Electrochem. Soc. 144 (1997) 2486–2490.
[5] M. Wainwright, M.N. Byrne, M.A. Gattrell, J. Photochem. Photobiol. B 96 (2006) 227–230.
[6] H. Obata, Bull. Chem. Soc. Jpn. 34 (1961) 1057–1063.
[7] A. Mills, J. Wang, J. Photochem. Photobiol. A: Chem. 127 (1999) 123–134.
[8] T. Snehalatha, K.C. Rajanna, P.K. Saoprakash, J. Chem. Educ. 74 (1997) 228–233.
[9] R. Aplin, T.D. Waite, Water Sci. Technol. 42 (2000) 345–354.
[10] F.S.G. Einschlag, J. Lopez, L. Carlos, A.L. Capparelli, A.M. Braun, E. Olivares, Environ. Sci. Technol. 36 (2002) 3936–3944.
[11] A.B. Prevot, C. Baiocchi, M.C. Brussino, E. Pramauro, P. Savarino, V. Augugliaro, G. Marci, L. Palmisano, Environ. Sci. Technol. 35 (2001) 971–976.
[12] C.M. Cho, J.H. Noh, I. Cho, J. An, K.S. Hong, J. Am. Ceram. Soc. 91 (2008) 3753–3755.
[13] T. Soltani, M.H. Entezari, Ultrason. Sonochem. 20 (2013) 1245–1253.
[14] T. Soltani, M.H. Entezari, Chem. Eng. J. 223 (2013) 145–154.
[15] N. Kakuta, J.M. White, A.J. Bard, A. Campion, M.A. Fox, S.E. Webber, M. Finlayson, J. Phys. Chem. 89 (1985) 48–52.
[16] S.V. Kalinin, M.R. Suchomel, P.K. Davies, D.A. Bonnel, J. Am. Ceram. Soc. 85 (2002) 3011–3017.
[17] S. Katz, P. McIntyre, C. Paul, McIntyre Research Group, McIntyre Group Webpage, Stanford University, 2013.
[18] Y.G. Wang, G. Xu, Z.H. Ren, X. Wei, W.J. Weng, P. Du, G. Shen, G.R. Han, J. Am. Ceram. Soc. 90 (2007) 2615–2617.
[19] S. Shetty, V.R. Palkar, R. Pinto, Pramana J. Phys. 58 (2002) 1027–1030.
[20] N. Das, R. Majumdar, A. Sen, H. Maiti, Mater. Lett. 61 (2007) 2100–2104.
[21] J. Wei, D. Xue, Y. Xu, Scr. Mater. 58 (2008) 45–48.
[22] G.D. Achenbach, W.J. James, R. Gerson, J. Am. Ceram. Soc. 8 (1967) 437–438.
[23] J.K. Kim, S.S. Kim, W.-J. Kim, Mater. Lett. 59 (2005) 4006–4009.
[24] C. Chen, J.R. Cheng, S.W. Yu, L.J. Che, Z.Y. Meng, J. Cryst. Growth 291 (2006) 135–139.
[25] G. Achenbach, W. James, R. Gerson, J. Am. Ceram. Soc. 8 (1967) 437–443.
[26] K. Mahesh, V. Palkar, K. Srinivas, S. Suryanarayana, Appl. Phys. Lett. 76 (2007) 2764–2766.
[27] R.N.P. Choudhary, D.K. Pradhan, G.E. Bonilla, R.S. Katiyar, J. Alloys Compd. 437 (2007) 220–224.
[28] F. Gao, Y. Yuan, K.F. Wang, X.Y. Chen, F. Chen, J.M. Liu, Appl. Phys. Lett. 89 (2006) 102506–102509.
[29] X.Y. Zhang, C.W. Lai, X. Zhao, D.Y. Wang, J.Y. Dai, Appl. Phys. Lett. 87 (2005) 1431021–2141023.
[30] M. Sivakumar, A. Towata, K. Yasui, T. Tuziuti, Y. Iida, Curr. Appl. Phys. 6 (2006) 591–593.
[31] N.K. Dhas, K.S. Suslick, J. Am. Chem. Soc. 127 (2005) 2368–2369.
[32] M.H. Entezari, N. Ghows, Ultrason. Sonochem. 18 (2011) 127–134.
[33] N. Ghows, M.H. Entezari, Ultrason. Sonochem. 17 (2010) 878–883.
[34] N. Ghows, M.H. Entezari, Ultrason. Sonochem. 18 (2011) 269–275.
[35] N. Ghows, M.H. Entezari, J. Hazard. Mater. 195 (2011) 132–138.
[36] N. Ghows, M.H. Entezari, Ultrason. Sonochem. 20 (2013) 386–394.
[37] J. Bartram, R. Balance, United Nations Environment Programme, E&FN Spon, an imprint of Chapman & Hall, London, UK, 1996.
[38] S. Ahmed, M.G. Rasul, R. Brown, M.A. Hashib, J. Environ. Manage. 92 (2011) 311–330.
[39] K.S. Suslick, S.B. Choe, A.A. Cichowlas, M.W. Grinstaff, Nature 353 (1991) 414–416.
[40] Z.F. Bian, Y.N. Huo, Y. Zhang, J. Zhu, Y.F. Lu, H.X. Li, Appl. Catal. B 91 (2009) 247–253.
[41] D.A. Chang, P. Lin, T.Y. Tseng, J. Appl. Phys. 77 (1995) 4445–4451.
[42] Y.N. Huo, Y. Jin, Y. Zhang, J. Mol. Catal. A: Chem. 331 (2010) 15–20.
[43] S. Kohtani, M. Koshiko, A. Kudo, et al., Appl. Catal. B 46 (2003) 573–586.
[44] Y. Galagan, W.F. Su, J. Photochem. Photobiol. A 195 (2008) 378–383.
[45] S.K. Kansal, M. Singh, D. Sud, J. Hazard. Mater. 141 (2007) 581–590.
[46] Z.F. Bian, Y.N. Huo, Y. Zhang, J. Zhu, Y.F. Lu, H.X. Li, Appl. Catal. B: Environ. 91 (2009) 247–253.
[47] M. Contineanu, C. Bercu, I. Contineanu, A. Neacsu, An. Univ. Bucuresti. Chimie. 18 (2009) 29–37.
[48] M. Misran, D. Matheus, P. Valente, A. Hope, Aust. J. Chem. 47 (1994) 209–216.
[49] D. Severino, H.C. Junquera, M. Gugliotti, D.S. Gabrielli, M.S. Baptista, J. Photochem. Photobiol. 77 (2003) 459–468.
[50] N. Takeda, T. Torimoto, S. Sampath, S. Kuwabata, H. Yoneyama, J. Phys. Chem. 99 (1995) 9986–9991.
[51] A. Mills, R.H. Davis, D. Worsley, Chem. Soc. Rev. 22 (1993) 417–425.
[52] J.-M. Herrmann, Catal. Today 53 (1999) 115–129.